Flow characterization of the VKI Longshot wind tunnel

Dr. Guillaume Grossir / Bruno Dias
Aeronautics and Aerospace department
von Karman Institute for Fluid Dynamics
Chaussée de Waterloo, 72
Rhode-Saint-Genèse, 1640
Belgium

grossir@vki.ac.be / bruno.ricardo.barros.dias@vki.ac.be

ABSTRACT

The VKI Longshot is a cold-hypersonic wind tunnel operating above Mach 10 at large free-stream unit Reynolds numbers using pure nitrogen. The determination of the free-stream flow properties in this facility relies on three probes: a Pitot, a stagnation point heat flux probe and a free-stream static pressure one. A short description of the probes and their instrumentation is provided. The free-stream flow characterization methodology is then given, i.e. detailing how the flow properties of interest are inferred from the few experimental inputs. The corresponding theoretical approach focuses on the free-stream region: it solves shock conservation equations in front of the Pitot probe, while accounting for high-temperature effects and possibly free-stream thermal non-equilibrium provided free-stream vibrational temperature measurements are made available. The Fay-Riddell equation is used to relate the total enthalpy to the stagnation point heat flux but alternative correlations may be implemented. Longshot free-stream values for the Mach number, static temperature, flow velocity and Reynolds number are cross-checked against experimental data from independent measurement techniques (Schlieren flow visualization, flow condensation experiments and boundary layer laminar-to-turbulent experiments). An excellent agreement is observed in all instances which demonstrates the accuracy of the theoretical approach used. The precision of the method is also quantified. The present rebuilding method is not restricted to nitrogen flows and can also be applied to hypersonic facilities operating at higher enthalpies.

Contents

NOMENCLATURE

Latin Symbols

a	speed of sound, $\mathrm{m/s}$
c	specific heat capacity, $\mathrm{J/(kg.K)}$
C	constant (Sutherland's equation), K
D	probe diameter, m
e	specific internal energy, $\mathrm{J/kg}$
E	specific total energy, $\mathrm{J/kg}$
h	specific flow enthalpy, $\mathrm{J/kg}$
$\mathcal{H}$	set of indices for heavy species, $-$
H_p	set of indices for molecules, $-$
k	thermal conductivity, $\mathrm{W/(m.K)}$
k_B	Boltzmann's constant, $1.806488 \cdot 10^{-23}\,\mathrm{J/K}$
L	probe length, m
Le	Lewis number, $-$
M	Mach number, $-$
M	Molar mass, $\mathrm{kg/mol}$
N_A	Avogadro constant, $1/\mathrm{mol}$
p	pressure, Pa
$\dot{P}$	Nozzle expansion rate parameter, $1/\mathrm{s}$
Pr	Prandtl number, $-$
p_{t_2}	Pitot pressure, Pa
$\dot{q}_f$	heat flux along a flat surface, $\mathrm{W/m^2}$
$\dot{q}_w$	stagnation point heat flux, $\mathrm{W/m^2}$
r	specific gas constant, $r_{N_2} = 296.80898\,\mathrm{J/(kg.K)}$
$\mathcal{R}$	universal gas constant, $\mathcal{R} = 8.3144621\,\mathrm{J/(K \cdot mol)}$
Re	Reynolds number, $-$
$\mathrm{Re}_{\mathrm{unit}}$	Reynolds number based on a $1\,\mathrm{m}$ reference length, $1/\mathrm{m}$
Re_x	Reynolds number based on a reference length x, $-$
R_N	nosetip radius, m
s	specific entropy, $\mathrm{J/(kg.K)}$
s	distance measured along the surface, from a sharp nosetip, m
$\mathcal{S}$	number of species in the mixture
t	time, ms
T	temperature, K
T_0	reference temperature, K
T_{el}	electronic temperature, K
T_{t_2}	stagnation temperature downstream a normal shock, K
T_v	vibrational temperature, K
u	flow velocity, $\mathrm{m/s}$
x	molar fraction, $-$

x, y	Cartesian coordinate, m
y	mass fraction, $-$

Greek Symbols

α	thermal diffusivity, m^2/s
γ	specific heat ratio, $-$
θ_{v_i}	characteristic vibrational temperature, K
μ	dynamic viscosity, $\mathrm{Pa.s}$
μ_0	reference dynamic viscosity, $\mathrm{Pa.s}$
ρ	density, kg/m^3

Subscripts

∞	free-stream value
D	based on a reference diameter D
eq	under equilibrium conditions
fr	under frozen conditions
i	for species i
i, n	indices
L	based on a reference length L
t	total quantity
w	at the wall

Superscripts

E	relative to electronic mode
R	relative to rotational mode
T	relative to translational mode
V	relative to vibrational mode

Abbreviations

ARD	Atmospheric Reentry Demonstrator
CARS	Coherent Anti-Stokes Raman Spectroscopy
IXV	Intermediate eXperimental Vehicle
LEO	Low Earth Orbit
LST	Linear Stability Theory
VKI	von Karman Institute

1.0 INTRODUCTION

The determination of free-stream flow properties has always represented a key part of wind tunnel experiments. This holds true with hypersonic facilities. In spite of decades of operation, it remains challenging to day due to numerous complex phenomena such as dense gas effects [1], high temperatures, or non-equilibrium effects [2–5], among others, which may occur and need to be accounted for. Difficulties are often stressed further by the short test time available in these facilities [6] and by limited instrumentation capabilities.

Similarity parameters (e.g. the free-stream Mach number, the free-stream Reynolds number...) need to be accurately determined in order to ensure a correct duplication of the flight conditions of interest. Besides, free-stream flow properties are often also used as reference values whenever dimensionless quantities (e.g. heat transfer, aerodynamic coefficients...) need to be expressed. This justifies the quest for accurate free-stream flow properties.

Unfortunately, most of the quantities of interest cannot be measured directly with dedicated probes. Instead, various rebuilding strategies [7–12] have been used over the years. Based on few measurements available, these theoretical methods determine, in a stepwise procedure and with various assumptions [13], additional flow properties from which quantities of interest can eventually be derived. The main drawbacks of these procedures are usually the limiting assumptions on which they rely, and the propagation of uncertainties which follows from the stepwise approach.

In the following, recent attempts to improve the flow characterization in the Longshot hypersonic tunnel are reported. Emphasis is placed on the flow characterization associated with the simulation of Earth reentries. The Longshot wind tunnel is first presented in §2.0. The different probes involved are then shortly described in §3.0. The theoretical methodology used to derive all flow properties of interest is described in §4.2, and represents an extension of the method introduced by Olivier [10]. Selected free-stream flow properties are then cross-validated using independent measurement techniques (§5.0). Uncertainties on free-stream flow properties are also reported.

2.0 THE VKI LONGSHOT GUN TUNNEL

2.1 Historical background

The VKI Longshot (illustrated in Fig. 1) is a unique worldwide hypersonic wind tunnel that has been designed in the early 1960s in the U.S. (at Republic Aviation [6]). It is especially aiming at aerothermodynamic investigations in high-speed flows as experienced during Earth reentries, i.e. at high Mach number and large Reynolds number. Since 1967, this wind tunnel is operated at the von Karman Institute for Fluid Dynamics (VKI), in Belgium [14, 15]. It is now established as a reference European wind tunnel for cold-hypersonic experiments within a perfect gas environment.

2.2 Fields of application

This facility has long been used for the generation of aerothermodynamic databases for reentry vehicles (e.g. Hermes, EXPERT, IXV...), for the aerothermodynamic characterization of space probes in either Earth or Martian environments (e.g. ARD, MSRO...), and more recently for aerothermodynamic measurements on typical space debris geometries. It is also used to address fundamental hypersonic phenomena (e.g. boundary layer laminar-to-turbulent transition, shock-waves/boundary-layer interactions, flap effectiveness...) on real and generic configurations (e.g. flat plates, cones, double cones, compression corners...).

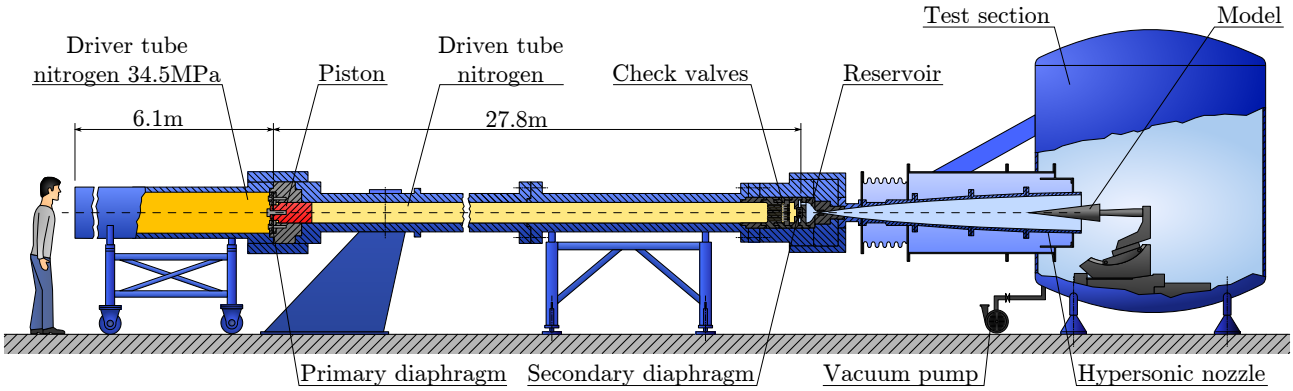

Figure 1: Sketch of the VKI Longshot hypersonic gun tunnel.

This facility has been regularly modified over the years in order to improve its performances, among others: new contoured nozzles (1990, 2019), testing using different gases (nitrogen, carbon dioxide), improved free-stream flow characterization using various free-stream diagnostic techniques... Since 2017, the facility is also semi-automated for improved safety, repeatability and efficiency.

2.3 Principle of operation

The VKI Longshot is based on the principle of a gun tunnel with an inertial piston used to compress the test gas up to moderate enthalpies, before expanding it through a hypersonic nozzle. Referring to Fig. 1, it is composed of the following main elements:

- a driver tube (initially filled with high pressure nitrogen, typically about $34.5\,\mathrm{MPa}$),
- a long driven tube (initially filled with the test gas near ambient pressure and temperature),
- a piston (initially located at the interface between the driver and the driven tubes; it prevents gas mixing between the two tubes and its kinetic energy is used to compress the test gas up to large stagnation pressures),
- 48 check valves at the end of the driven tube (they are used to trap the gas in the following reservoir once peak stagnation conditions are generated),
- a nozzle (either a contoured or a conical one),
- a test section (evacuated prior to an experiment, and in which instrumented models and probes are located),
- and two diaphragms: a primary one attached to the piston, and a secondary one isolating the driven tube from the reservoir.

The compression process of the Longshot has been described in details elsewhere [16–18]. Upon the controlled rupture of a primary diaphragm, the piston is set free and accelerated by the high pressure driver gas down the driven tube. It is rapidly reaching supersonic velocities and compresses almost adiabatically the test gas located ahead. Shock waves and the kinetic energy of the piston contribute to increase the internal energy of

the test gas and generate peak pressures and temperatures in the reservoir on the order of $400\,\mathrm{MPa}$ and $2500\,\mathrm{K}$. The 48 check valves located by the end of the driven tube are automatically closed as these peak stagnation conditions are achieved and prevent the compressed gas from flowing back again to the driven tube. The test gas is then expanded through a nozzle. Thanks to the check valves, the useful test time is enlarged by at least an order of magnitude with respect to the conventional gun tunnel design (hence the *Long*shot denomination for this wind tunnel, with typically about $20\,\mathrm{ms}$ of useful test time).

2.4 Typical flow conditions

Different stagnation flow conditions can be generated by altering the mass of the piston and the initial driven tube pressure (among other parameters [18]). Specific total enthalpies are commonly limited to $2.5\,\mathrm{MJ/kg}$.

Upon expansion through a nozzle, the flow reaches moderate velocities (on the order of $2200\,\mathrm{m/s}$) which, in combination with low free-stream static temperatures (on the order of $50 - 80\,\mathrm{K}$), contribute to generate large Mach numbers in the free-stream. This principle of operation is shared by other cold-hypersonic wind tunnels but the uniqueness of the Longshot is to combine high Mach numbers with the large Reynolds numbers associated with typical reentry trajectories (Fig. 2). The duplication of these similarity parameters represents the basics of aerothermodynamic investigations.

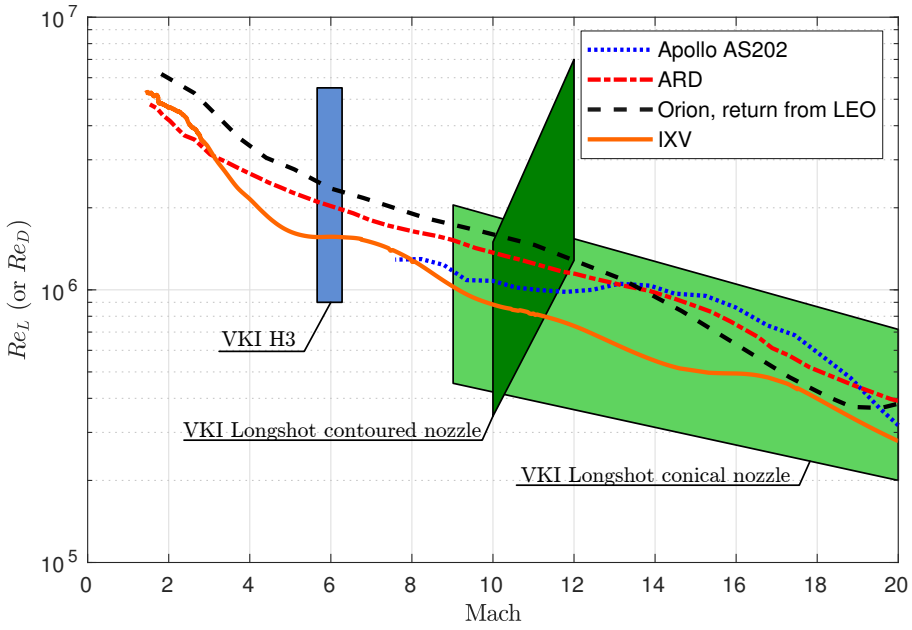

Figure 2: Operational map of the VKI Longshot compared to typical reentry trajectories.

Pure nitrogen (instead of air) is used as a test gas in the Longshot whenever considering Earth reentries. Given the moderate flow enthalpies generated this prevents dissociation from taking place, and enables aerothermodynamic investigations to be performed in a reference perfect gas environment (i.e. ideal for the validation of numerical codes).

Another peculiarity of the Longshot tunnel is that a finite amount of gas is compressed in a constant volume reservoir [18]. This leads to a temporal decay of the stagnation conditions during a run as the gas flows through the nozzle throat. Interestingly, this allows to scan a range of Reynolds numbers during a single test run and contributes to increase the productivity of the wind tunnel.

The flow establishment time along most models remains sufficiently short with respect to the characteristic time of the flow so that Longshot experiments can be viewed as a series of quasi-steady flow configurations [19].

3.0 PROBES

Three intrusive probes used for the Longshot flow characterization are described hereafter. They are used to measure the Pitot pressure (§3.1), the heat flux at the stagnation point of a hemispherical probe (§3.2), and the free-stream static pressure (§3.3).

3.1 Pitot probe

Among the Pitot probes regularly used for Longshot flow characterization is the one illustrated in Fig. 3. The outer diameter of the probe is $15\,\mathrm{mm}$ and the overall length is $130\,\mathrm{mm}$. The head of the probe follows a $30\,^\circ$ half-angle cone in order to deflect eventual flow seeding material away from the stagnation point. The tip of the head is truncated and a $1\,\mathrm{mm}$ diameter tube leads to an absolute fast-response piezo-resistive pressure transducer (Kulite XCQ-093).

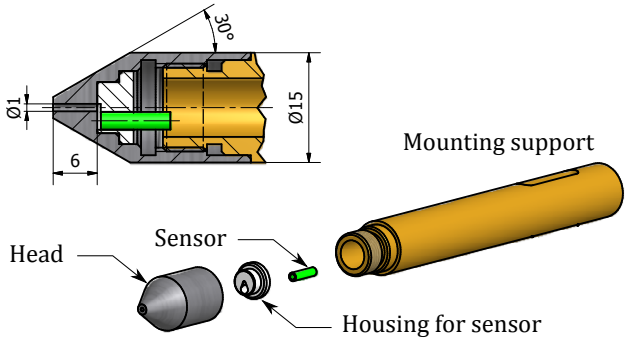

Figure 3: Schematic of a typical Longshot Pitot probe.

3.2 Stagnation point heat flux probe

The probe illustrated in Fig. 4 is used to measure the transient stagnation point heat flux. It is composed of a fast-response coaxial type-E thermocouple (Chromel-Constantan), manufactured by the Shock Wave Laboratory [20] (RWTH Aachen University, Germany). It is flush-mounted at the nosetip and shaped to match the curvature radius of the hemispherical head. The diameter of the active junction of the thermocouple is $0.5\,\mathrm{mm}$. In order to ensure a 1-dimensional heat flux through the thermocouple, a Chromel insert with identical thermal properties surrounds the sensor.

The stagnation point heat flux is retrieved by integrating the temperature history according to eq. 1. This equation is strictly valid only for a 1-dimensional heat flux into a semi-infinite body of uniform and constant thermal properties ρck [21].

$$\dot{q}_f(t_n) = 2\sqrt{\frac{\rho ck}{\pi}} \sum_{i=1}^{n} \frac{T_w(t_i) - T_w(t_{i-1})}{\sqrt{t_n - t_i} + \sqrt{t_n - t_{i-1}}} \tag{1}$$

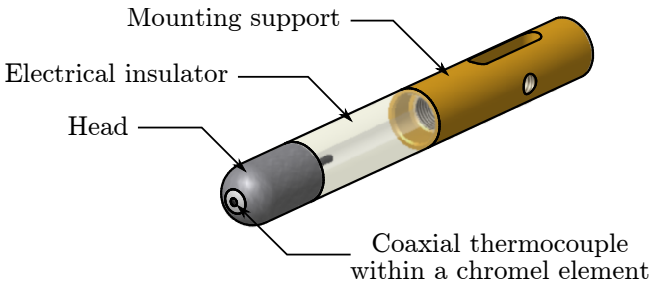

Figure 4: Stagnation point heat flux probe.

The penetration depth, where the local temperature and heat fluxes are 1% of the values at the front surface, can be conservatively approximated by $y = 4\sqrt{\alpha t}$ [21]. In the Longshot wind tunnel, with a typical 20 ms test time, a minimum thickness of 1.3 mm is sufficient for the thermocouples to respect the semi-infinite assumption. This is ensured by the present design and the surrounding Chromel insert. Corrections for radial conduction effects are accounted for following eq. 2 [22]:

$$\dot{q}_w(t_n) = \dot{q}_f - \frac{k\sigma}{2R_N}\left(T_w - T_i\right) \tag{2}$$

where $\dot{q}_f$ is the heat flux obtained form eq. 1 corresponding to the heat flux on a flat surface, k is the thermal conductivity of the material, $\sigma = 2$ in the case of spherical surface, R_N is the radius of curvature of the surface, and T_i is the initial surface temperature.

3.3 Free-stream static pressure probe

3.3.1 Probe design and instrumentation

A slender probe (Fig. 5) is used to measure the free-stream static pressure in the Longshot wind tunnel. The design of this probe is based on the one presented by [23].

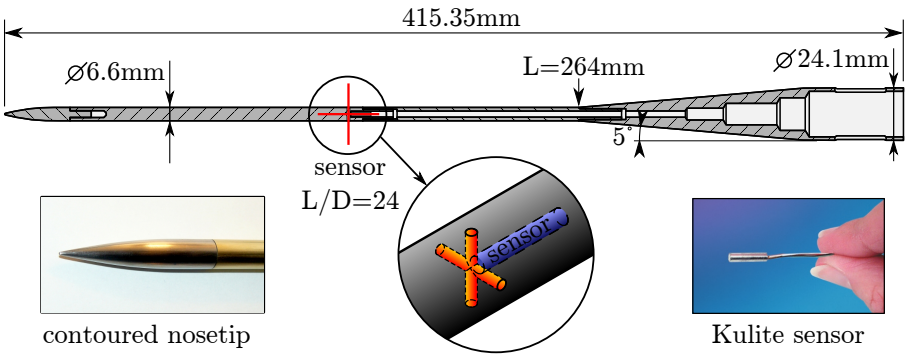

Figure 5: Schematic of the Longshot free-stream static pressure probe.

The contoured nose has an aspect ratio of 4.5 and is composed of a 10° half-angle cone followed by a 4^{th} order polynomial smoothly connecting to the cylindrical part of the probe. The nosetip is slightly blunted with $R_N = 0.053\,\text{D}$ in order to minimize the local heat transfer and to ease the machining [19, 24].

The cylindrical body of the probes is hollow and houses one absolute fast-response pressure sensor (Kulite XCQ-093-0.35bar) at a length to diameter ratio of $^{L}/_{D} = 24$. Four holes ($\varnothing 0.6\,\mathrm{mm}$) are drilled through the cylindrical body at $90\,^{\circ}$ circumferential angles and lead to an internal miniature cavity where is located the pressure sensor. The small size of the cavity ensures a good response time of the probe in the short duration Longshot facility. The sensor is calibrated at low pressure against a reference MKS Baratron 626C sensor. A non-linear calibration law is used for better accuracy.

Special attention was paid to the surface quality along the body of the probe, in order to avoid disturbances such as gaps or burrs (apart from the orifices) that might perturb the development of the boundary layer. The conical base of the probe starts at $^{L}/_{D} = 40$, far downstream of the sensor locations to avoid any upstream influence of flow recirculation near the base corner. In addition, the opening half-angle of the base is only $5\,^{\circ}$ to limit the extension of this flow separation region. This conical support transitions to a cylinder of diameter $3.65D$, required to adequately fix the probe in the VKI Longshot test section.

3.3.2 Prediction of the viscous effects along the probe

The viscous effects taking place along the probes have been evaluated numerically for different free-stream conditions (Fig. 6). The pressure ratio $^{p_w}/_{p_\infty}$ at $^{L}/_{D} = 24$ is found to be slightly smaller than unity for the Longshot operating conditions [19, 25].

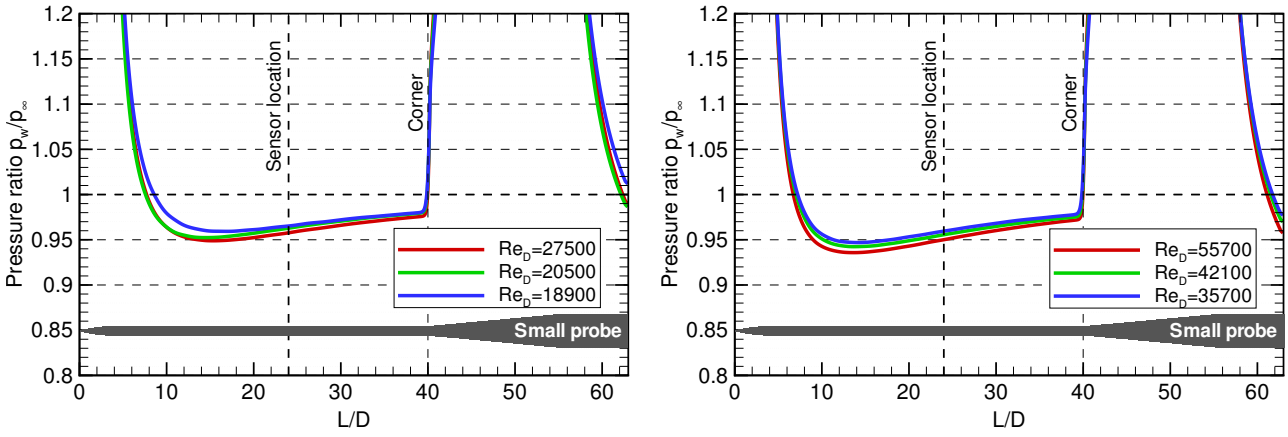

(a) Low Reynolds.

(b) Medium Reynolds.

Figure 6: Wall pressure distribution along the static pressure probe (numerical results) for different free-stream conditions [25].

Another static pressure probe, equipped with several sensors along its axis, has been used to confirm the streamwise pressure distribution. Experimental results compare favorably against numerical predictions [19] and show that only weak viscous effects are induced by the large Reynolds number Longshot flow. The unlikely departure from laminar boundary layers along the probe has also been shown to have a negligible influence on the viscous correction [25].

4.0 LONGSHOT FREE-STREAM FLOW CHARACTERIZATION

4.1 Flowchart and overview of the free-stream rebuilding methodology

4.1.1 Experimental inputs

The determination of the free-stream flow properties relies on three experimental measurements, all performed within the test section, as recommended by [10]:

- the Pitot pressure p_{t_2} (with the probe described in §3.1),
- the stagnation point heat flux $\dot{q}_w$ on a hemispherical probe (with the probe described in §3.2),
- and the free-stream static pressure p_∞ (with the probe described in §3.3).

Measurements or estimations of the free-stream vibrational temperature T_v can also benefit the accuracy of the method. The reservoir pressure p_0 may be monitored but is nowhere involved in the determination of free-stream conditions.

4.1.2 Flowchart

The procedure followed is illustrated in Figs. 7 and 8 which both support the subsequent description. The numerical code is coupled with the VKI *Mutation* library developed by [26], enabling the computation of transport and thermodynamic properties of gases at high temperature including chemical equilibrium or finite-rate chemistry. It will be shown that this method accounts for high-temperature effects (e.g. vibrational excitation, dissociation...), rigorously solves shock conservation equations and handles free-stream thermal non-equilibrium.

Referring to Fig. 8, the aim is to find two of the unknown free-stream quantities (the velocity u_∞, and the static temperature T_∞) which provide a satisfactory set of free-stream conditions to match the measured stagnation point heat flux $\dot{q}_w$ on a hemispherical probe, and the Pitot pressure p_{t_2}. As intermediate steps, conservation equations for a thermal non-equilibrium mixture are solved across a normal shock wave; stagnation conditions in the post-shock region are derived assuming an adiabatic and isentropic compression; and the Fay-Riddell equation is used to determine the heat transfer rate at the tip of a hemispherical probe based on boundary layer edge stagnation flow conditions. Iterative processes are involved until convergence is achieved to a prescribed degree of accuracy.

4.1.3 Theoretical assumptions

The present methodology focuses on the free-stream region. Unlike approaches used elsewhere [7–9, 11, 12], it is therefore not required to describe the gas in the reservoir nor during the nozzle expansion. This simplifies the analysis since real gas equations of state and assumptions for an adiabatic/isentropic flow expansion are no longer needed.

Intermolecular forces are negligible, both in the free-stream and in the high-temperature shock layer. The simple (thermally) perfect gas equation of state, which holds true in presence of vibrational excitation, is therefore sufficiently accurate.

Park has shown that the number of collisions required to reach equilibrium between the rotational and translational modes of nitrogen steadily increases with temperature [27, 28]. At temperatures lower than $12\,000\,\mathrm{K}$, the rotational-translational relaxation is faster than the vibrational-translational relaxation. For the Longshot facility, where temperatures are usually lower than $2500\,\mathrm{K}$, the gas translational temperature is assumed to be

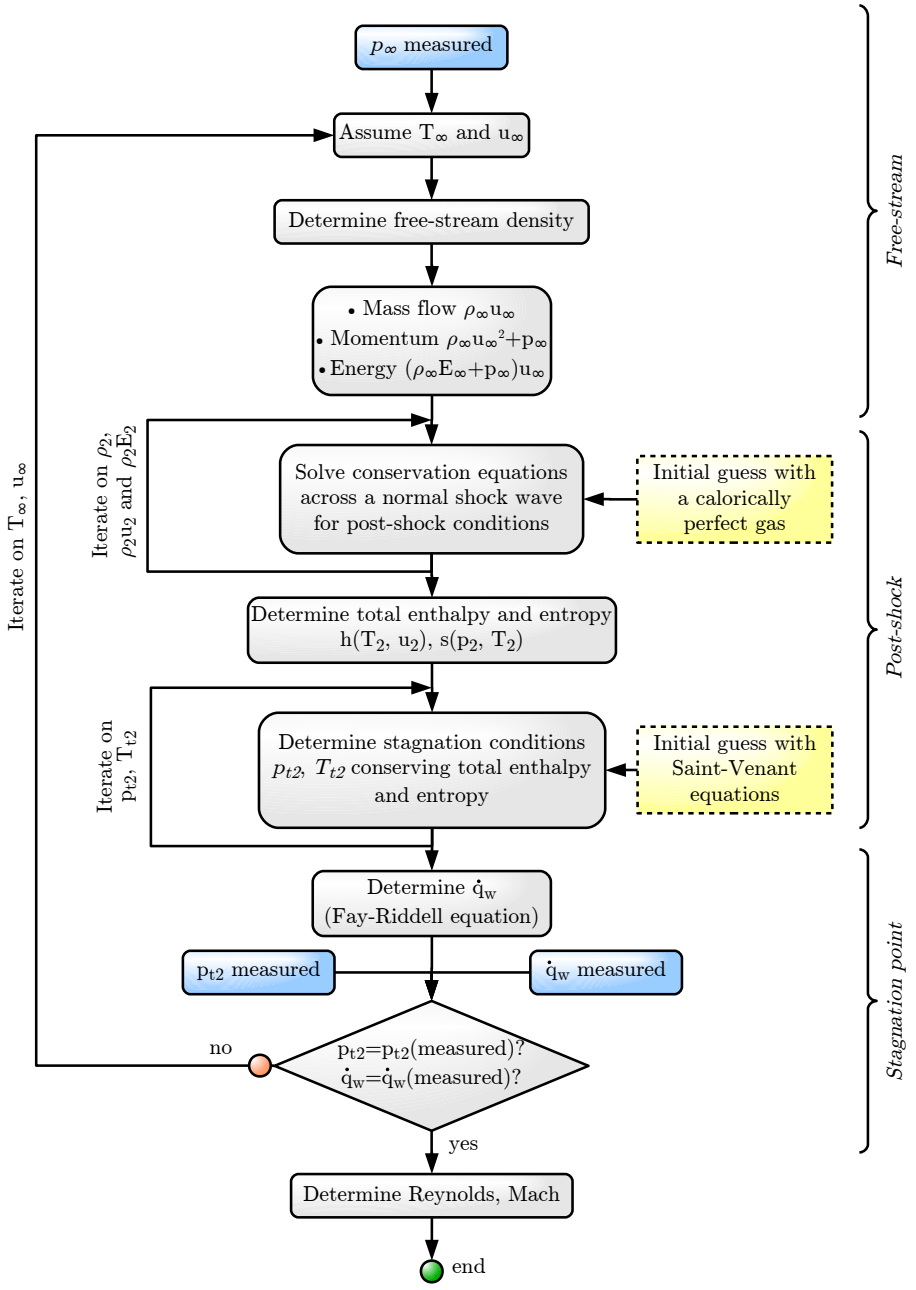

Figure 7: Flowchart of the free-stream rebuilding procedure implemented for the VKI Longshot hypersonic wind tunnel.

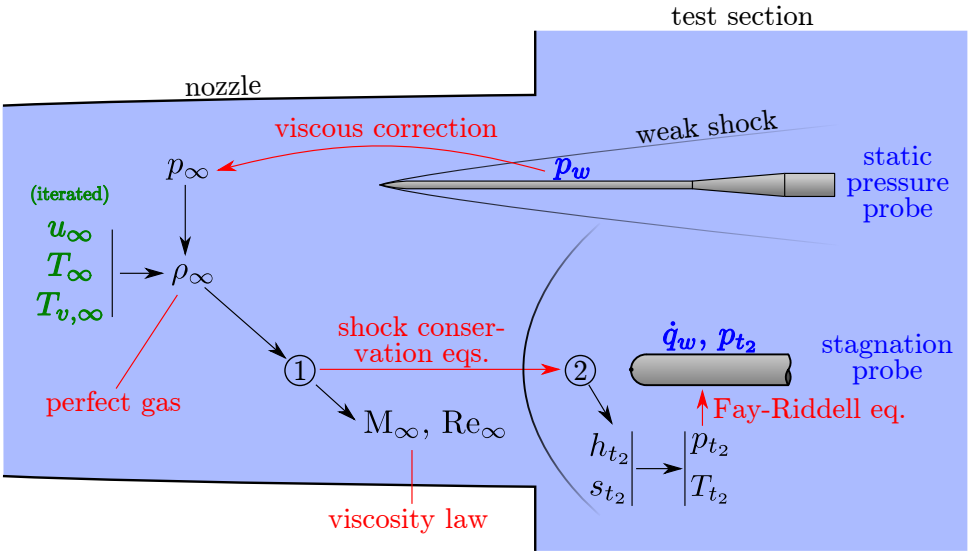

Figure 8: Schematic of the rebuilding procedure implemented for the VKI Longshot hypersonic wind tunnel. Not to scale for clarity.

in equilibrium with the rotational one. On the other hand, the vibrational temperature may differ from the translational temperature due to rapid nozzle expansion and the insufficient number of collisions [2, 4]. The present rebuilding approach can account for these thermal non-equilibrium effects provided the free-stream vibrational temperature is supplied, or assumes free-stream equilibrium by assuming that the vibrational temperature is equal to the translational one.

The Fay-Riddell equation [13] is used to relate free-stream conditions to the stagnation point heat flux on a hemispherical probe. This equation was developed for air or a similar mixture and the present methodology is therefore restricted to similar species. A wider variety of gas mixtures could be accounted for providing this equation is replaced by a suitable one or by a numerical model. The shock layer flow, along the stagnation line, is assumed to slow down isentropically and to remain in thermal equilibrium.

4.2 Detailed methodology

The physico-chemical models used by the present method will be described first. This is followed by the descriptions of conservation equations across a normal shock, and of the Fay-Riddell equation.

4.2.1 Physico-chemical models

4.2.1.1 Chemical equilibrium

A gas mixture is first selected among the ones available in the *Mutation* library. For the pure nitrogen flow of the VKI Longshot wind tunnel, a nitrogen mixture with 5 species (N_2, N, N_2^+, N^+, e^-) is considered, even though dissociation and ionization are not expected. The composition (molar fractions x_i) of the mixture is then determined by the *Mutation* library assuming chemical equilibrium, based on equilibrium constants, for a prescribed static pressure and temperature, i.e:

$$x_i = f\left(p, T, T_v, T_{el}\right), \quad i \in \mathcal{S}, \tag{3}$$

where $\mathcal{S}$ is the number of species in the mixture considered, with i representing each gas constituent and $\sum_{i \in \mathcal{S}} x_i = 1$. The charge of the mixture is assumed to be equal to zero.

Based on the equilibrium composition of the mixture, other properties of interest such as the flow density ρ_∞, can also be derived:

$$\rho = \sum_{i \in \mathcal{S}} x_i \frac{M_i}{N_A} n \tag{4}$$

where N_A is the Avogadro constant and M_i the molar mass of each species. The number density n, is determined from the local pressure and temperature according to:

$$n = \frac{p}{k_B T} \tag{5}$$

where k_B is the Boltzmann constant.

The perfect gas equation of state is extended to a mixture using a linear mixture rule as in eq. 6 which then takes into account the mass fraction y of every species present.

$$p = \sum_{i \in \mathcal{H}} \frac{y_i}{M_i} \rho \mathscr{R} T + \frac{y_e}{M_e} \rho \mathscr{R} T_e \tag{6}$$

where $\mathscr{R}$ is the universal gas constant and $\mathcal{H}$ stands for the set of heavy species (atoms and molecules).

4.2.1.2 Thermodynamic properties

The internal energy for the gas mixture is determined from the results of statistical thermodynamics for high-temperatures gases [29]. The translational, rotational, vibrational, electronic and formation energies are expressed according to the following equations for every species present:

$$e_i^T(T) = \frac{3}{2} r_i T, \quad i \in \mathcal{S}, \tag{7}$$

$$e_i^R(T) = \frac{\mathfrak{L} r_i T}{2}, \quad i \in H_p, \tag{8}$$

$$e_i^V(T_v) = \sum_m \frac{r_i \theta_{i,m}^V}{e^{\theta_{i,m}^V / T_v} - 1}, \quad i \in H_p, \tag{9}$$

$$e_i^E(T_{el}) = f(T_{el}), \quad i \in \mathcal{H}, \tag{10}$$

$$e_i^F(T) = \mathrm{C}_i, \quad i \in \mathcal{S}, \tag{11}$$

where the symbol H_p is the set of indices for molecules, r_i is the specific gas constant for every species considered and defined by $r_i = \frac{\mathscr{R}}{M_i}$, $\mathfrak{L} = 2$ for linear molecules and $\mathfrak{L} = 3$ otherwise. The quantity $\theta_{i,m}^V$ corresponds to the characteristic vibrational temperature associated to the vibrational mode m ($\theta^V = 3\,392.7\,\mathrm{K}$ for the single mode of N_2).

The internal energy of the species is obtained by summing the individual contributions of eqs. 7 to 11:

$$e_i = e_i^T + e_i^R + e_i^V + e_i^E + e_i^F, \quad i \in \mathcal{S}, \tag{12}$$

and the internal energy of the mixture is obtained from:

$$e = \sum_{i \in \mathcal{S}} y_i e_i \tag{13}$$

The total energy E of the flow follows from the internal energy e (eq. 13) and the kinetic energy contribution:

$$E = e + \frac{1}{2}u^2 \tag{14}$$

The enthalpy for all species can be obtained individually from their internal energy (eq 12):

$$h_i(T) = e_i + p_i/\rho_i, \quad i \in \mathcal{S}, \tag{15}$$

and the static enthalpy of the flow is obtained by:

$$h = \sum_{i \in \mathcal{S}} y_i h_i \tag{16}$$

The total enthalpy of the flow is the sum of this static enthalpy and the kinetic energy:

$$h_t = h + \frac{u^2}{2} \tag{17}$$

The entropy of the flow is determined by the *Mutation* library following the implementation given by [30], and is a function of temperature and pressure: $s = f(T, p)$.

4.2.1.3 Transport properties

Transport properties such as viscosity, thermal conductivity and diffusion coefficients are difficult to measure experimentally, especially at high temperatures. Kinetic theory, based on Boltzmann equation, provides an alternative link to compute such properties due to exchange of energy and momentum during a linear collision of particles. By accessing the interaction potentials or the cross-sections from experimental measurements, macroscopic properties are derived from the elastic collision of particles [30].

Multicomponent transport coefficients, derived from kinetic theory, are expressed as the solution of linear systems. The size of these linear systems is proportional to the number of species. By solving such linear systems, the viscosity of a mixture, depending on local temperature and pressure, can be determined ($\mu = \mu(p, T)$). The bulk viscosity of the gas is not considered in the present analysis, assuming that inelastic collisions are negligible.

4.2.1.4 Additional quantities of interest

Based on the quantities available either in the free-stream or in the post-shock region, additional quantities of interest can be derived. Among the ones widely used are the free-stream Reynolds number and the free-stream Mach number. They are determined as follow.

The free-stream unit Reynolds number based on a length of $1\,\mathrm{m}$ follows from eq. 18 using the free-stream viscosity μ_∞ estimated from the *Mutation* library.

$$\mathrm{Re}_{\text{unit},\,\infty} = \frac{\rho_\infty u_\infty}{\mu_\infty} \tag{18}$$

The Mach number is by definition the ratio of the local flow velocity and the local speed of sound. Depending on whether frozen or equilibrium chemical reactions are considered in the gas mixture, different expressions can be used for the speed of sound.

By definition, this quantity is $a = \left(\frac{\partial p}{\partial \rho}\right)_s$. This derivative can be performed assuming the composition of the mixture does not change in the internal structure of the sound wave, leading to the *frozen* speed of sound a_{fr}. Alternatively, an *equilibrium* speed of sound a_{eq} can be defined by assuming that the composition varies locally due to temperature and pressure variations within the sound wave. The resulting derivations for a frozen and an equilibrium speed of sound are respectively given as follows [31, 32]:

$$a_{fr}^2 = \gamma_{fr} r T \tag{19}$$

$$a_{eq}^2 = \gamma_{eq} r T \frac{1 - \frac{\rho^2}{p}\left(\frac{\partial e}{\partial \rho}\right)_T}{1 - \rho\left(\frac{\partial h}{\partial p}\right)_T} \tag{20}$$

where γ_{fr} is the ratio of frozen specific heats in a frozen mixture, and γ_{eq} is the ratio of equilibrium specific heats determined by including the effects of chemistry on the flow enthalpy and energy.

If chemistry effects take place, these two expressions can have significantly different values [31]. For the present case with the VKI Longshot tunnel, no dissociation is expected (even within the shock layer) so that the two values are identical. The evaluation of the speed of sound is nevertheless based on eq. 20 so that the processing method is as general as possible.

The free-stream Mach number M_∞ is finally determined from eq. 21 based on the equilibrium speed of sound in the free-stream $a_{eq,\infty}$.

$$M_\infty = \frac{u_\infty}{a_{eq,\infty}} \tag{21}$$

4.2.2 Rankine-Hugoniot jump conditions

Using the physico-chemical models described earlier, the determination of free-stream flow properties is achieved as follows.

The free-stream static pressure is the first experimental input required. Its measurement is achieved using the probe described in §3.3. Viscous interactions are corrected for using transfer functions derived from numerical results, as described by [25]. For the probing location at $\frac{L}{D} = 24$, the transfer function relating the static pressure measured along the probe to the free-stream one is nearly constant ($0.950 < \frac{p_w}{p_\infty} < 0.965$) over the whole range of the VKI Longshot flow conditions.

Initial guesses for the free-stream static temperature T_∞ and velocity u_∞ are then selected. The associated free-stream vibrational temperature can also be specified (providing this measurement is available), forced to an arbitrary value, or assumed equal to the free-stream static temperature[1] The chemical composition of the free-stream is then evaluated using eq. 3. The free-stream density follows from eq. 4 and the total energy of the flow is obtained from eq. 14.

[1]For the Longshot wind tunnel, it is assumed that the free-stream is in thermal equilibrium, i.e. the vibrational temperature T_v is equal to the rotational temperature T_r. Vibrational temperature measurements are needed to confirm or reject this hypothesis. The results presented in §5.0 indicate that the present thermal equilibrium assumption is likely correct. It does not imply however that the flow is in thermal equilibrium throughout the nozzle.

Conservation equations across a normal shock wave (namely the Rankine-Hugoniot jump conditions) can then be expressed, relating flow properties upstream and downstream a normal shock wave. These conservation equations are written as:

$$\rho_\infty u_\infty = \rho_2 u_2 \quad \text{(mass flow)} \tag{22}$$

$$p_\infty + \rho_\infty u_\infty^2 = p_2 + \rho_2 u_2^2 \quad \text{(momentum)} \tag{23}$$

$$(\rho_\infty E_\infty + p_\infty) u_\infty = (\rho_2 E_2 + p_2) u_2 \quad \text{(energy)} \tag{24}$$

This system of three equations contains four unknowns (i.e. ρ_2, u_2, p_2 and E_2 in the post-shock region) and cannot be solved without the addition of a fourth equation. The perfect gas equation of state is used for this purpose (eq. 6). A first solution of the system is obtained for a calorically perfect gas. The system is then solved for a thermally perfect gas using a Newton-Raphson method for non-linear equations, yielding a solution to the four unknown flow quantities in the post-shock region.

4.2.3 Shock layer and stagnation point (Fay-Riddell equation)

The set of free-stream conditions was based on initial guesses of the free-stream temperature and free-stream velocity. Whether these values are correct or not is evaluated by comparing the predicted stagnation point heat flux $\dot{q}_w$ and Pitot pressure p_{t_2} to the experimental measurements. To this end, stagnation conditions (Pitot pressure p_{t_2} and total temperature T_{t_2}) are sought in the following.

The gas is assumed to remain in thermal equilibrium in the shock layer and to be slowed down adiabatically and isentropically along the stagnation line. A first approximation for the Pitot pressure p_{t_2} and stagnation temperature T_{t_2} can be obtained by neglecting high-temperature effects and using Saint-Venant equations. High-temperature effects are then accounted for by solving eqs. 25 and 26. Another Newton-Raphson method is used for this iterative process.

$$h(T_{t_2}, p_{t_2}) = h(T_2, p_2) + \frac{u_2^2}{2} \tag{25}$$

$$s(T_{t_2}, p_{t_2}) = s(T_2, p_2) \tag{26}$$

The total pressure p_{t_2} will be compared later on with the experimental input. Besides, the total temperature T_{t_2} is not easily measured practically and the measurement of the heat flux at the stagnation point of a hemispherical probe has been usually preferred [33]. The Fay-Riddell equation (eq. 27) provides a theoretical model to relate the stagnation enthalpy (or the total temperature) to the stagnation point heat flux $\dot{q}_w$, for air and nitrogen mixtures. For the specific case of the VKI Longshot, no chemical reactions are expected because of the moderate temperatures reached, so that the Lewis number equals 1. This leads to some simplifications to the original equation and yields eq. 28. The nomenclature for the symbols and subscripts used is given in figure 9.

$$\dot{q}_w = 0.763 \times \mathrm{Pr}^{-0.6} \left(\rho_w \mu_w\right)^{0.1} \left(\rho_s \mu_s\right)^{0.4} \left[1 + \left(\mathrm{Le}^{0.52} - 1\right) \left(\frac{h_D}{h_s}\right)\right] (h_s - h_w) \sqrt{\left(\frac{du}{dy}\right)_s} \tag{27}$$

$$\dot{q}_w = 0.763 \times \mathrm{Pr}^{-0.6} \left(\rho_w \mu_w\right)^{0.1} \left(\rho_s \mu_s\right)^{0.4} (h_s - h_w) \sqrt{\left(\frac{du}{dy}\right)_s} \tag{28}$$

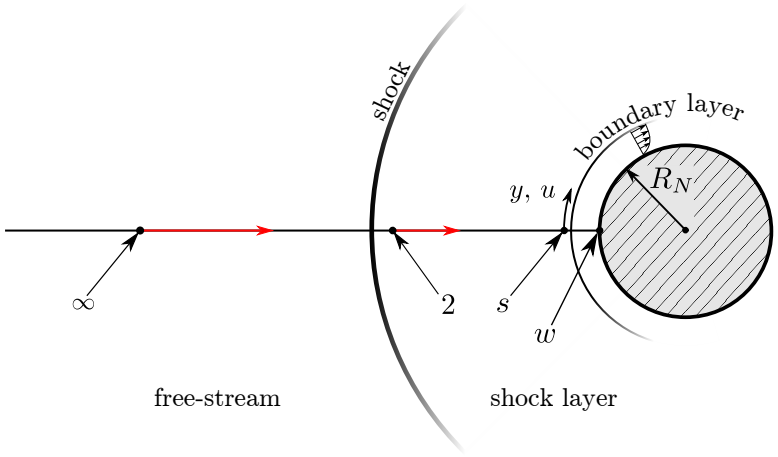

Figure 9: Nomenclature used by the Fay-Riddell equation.

The density at the wall ρ_w is computed from the Pitot pressure p_{t_2} and the measured wall temperature T_w at the stagnation point. The enthalpy at the wall h_w is obtained from eq. 16. The viscosity at the wall μ_w and the one corresponding to stagnation conditions at the edge of the boundary layer (μ_s) are determined from Sutherland's formula (eq. 29) since the Fay-Riddell equation was derived in that way:

$$\mu = \mu_0 \frac{T_0 + C}{T + C} \left(\frac{T}{T_0} \right)^{1.5} \tag{29}$$

where $\mu_0 = 17.81 \cdot 10^{-6}$ Pa.s, $T_0 = 300.55$ K and $C = 111$ K for nitrogen.

Stagnation quantities taken at the edge of the boundary layer are referred to by the subscript s. The stagnation density ρ_s is determined from stagnation conditions $p_{t_2} = p_s$ and $T_{t_2} = T_s$ using eq. 4 (only moderate densities are expected in the shock layer so that a perfect gas law is well suited).

Finally, the velocity gradient at the stagnation point is obtained from the modified Newtonian theory which reads:

$$\left(\frac{du}{dy} \right)_s = \frac{1}{R_N} \sqrt{\frac{2\left(p_s - p_\infty\right)}{\rho_s}} \tag{30}$$

where R_N is the nosetip radius of the hemispherical probe. Alternative correlations for velocity gradients could be used in higher-temperature environments [34, 35]. Yet, eq. 30 has been shown to provide the best agreement with numerical and experimental results [36] within the Longshot low-enthalpy environment and is therefore used in the present method.

4.2.4 Inverse problem (iterating on free-stream quantities)

The predicted Pitot pressure p_{t_2} and stagnation point heat flux $\dot{q}_w$ resulting from the initial choice of free-stream conditions are finally compared to the experimental inputs. A Newton-Raphson method is used until convergence is achieved on the free-stream unknowns u_∞ and T_∞. The free-stream, post-shock and stagnation point regions are then all characterized.

4.3 Validation of the numerical implementation

The validation of the present numerical implementation is achieved against the original method from Olivier [10]. The "medium" Reynolds number operating condition of the VKI Longshot wind tunnel is selected for this purpose, presenting flow conditions where only moderate high-temperature effects are expected, and with a negligible amount of dissociated species.

The Pitot pressure p_{t_2}, the stagnation point heat flux $\dot{q}_w$, and the free-stream static pressure p_∞ (including corrections [25] for viscous effects with $\frac{p_w}{p_\infty} = 0.959$) are used as experimental inputs. For better comparison purposes, the present method assumes free-stream thermal equilibrium ($T_v = T_\infty$). Both approaches use the same expression for the stagnation point velocity gradient (eq. 30) and both rely on viscosities from the *Mutation* library, except for the evaluation of the Fay-Riddell formula where the original Sutherland equation is used. The free-stream is assumed to be in thermal equilibrium.

Free-stream Mach and unit Reynolds numbers, derived by the end of the rebuilding process, are useful quantities considered for this validation. These flow properties are reported in Fig. 10 over the typical 20 ms test duration of the VKI Longshot tunnel.

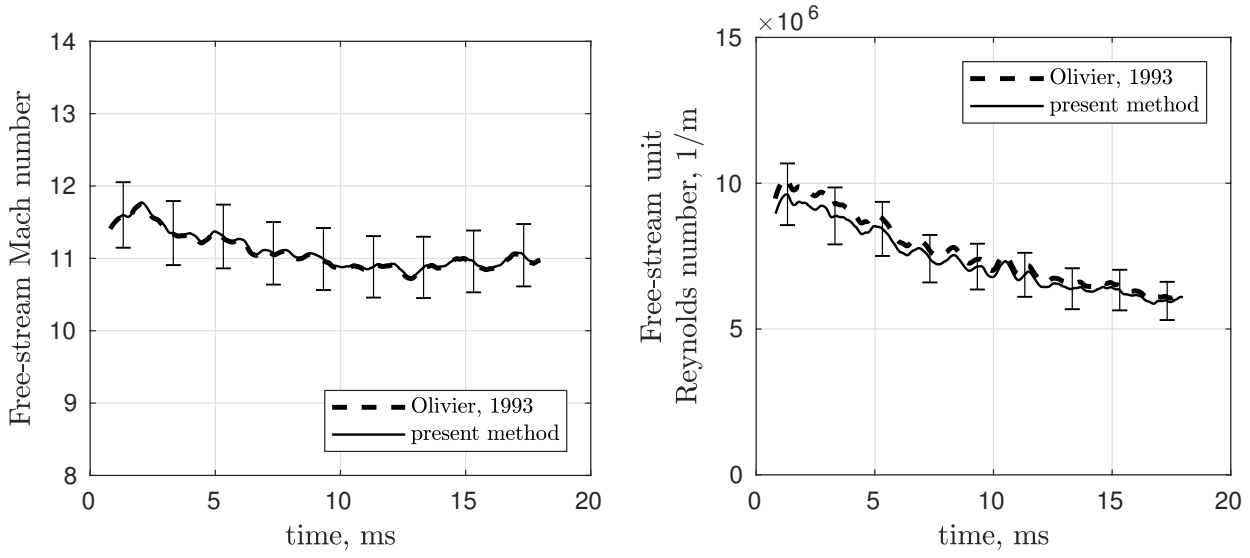

(a) Free-stream Mach number.

(b) Free-stream unit Reynolds number.

Figure 10: Validation of the present approach by determining free-stream conditions in the short duration VKI Longshot tunnel and comparing results to the ones obtained using the methodology from [10].

Both approaches yield the same free-stream Mach number (Fig. 10a). This is expected since this quantity is essentially driven by the ratio of static pressure (p_∞) to Pitot pressure (p_{t_2}), which are identical experimental inputs to both rebuilding methodologies.

The free-stream unit Reynolds number (Fig. 10b) also exhibits a close agreement between both methodologies. The temporal decay observed on this quantity is inherent to the working principle of the VKI Longshot wind tunnel following the expansion of a finite amount of gas from a constant volume reservoir. Differences observed on the free-stream unit Reynolds number are attributed to the excitation of vibrational modes in the shock layer, a phenomenon not accounted for by the earlier methodology [10]. The better match between both methods by the end of the test window is explained by the fact that the free-stream stagnation temperature decays from about 2100 K to 1100 K over the time window considered, hence with a lower excitation of vi-

brational energy in the shock layer by the end of the test time. Overall, discrepancies remain smaller than the uncertainties derived for this quantity.

The present approach and its numerical implementation are therefore regarded as validated.

5.0 CROSS-VALIDATION OF FREE-STREAM FLOW PROPERTIES

In the following, several experimental results obtained recently in the Longshot serve to indirectly estimate specific free-stream flow properties and therefore contribute to cross-validate the values determined from the theoretical rebuilding approach. The excellent agreement generally observed supports the accuracy of this free-stream rebuilding methodology.

5.1 Free-stream Mach number

Using the oblique shock wave theory [37], it is possible (for any given specific heat ratio γ) to relate the shock angle θ to the Mach number M and the deflection angle δ. As illustrated in Fig. 11, shock waves at hypersonic Mach numbers always lay close to the body and the sensitivity of the shock angle to the free-stream Mach number is weak (considering axisymmetric flows offers even less sensitivity [38]). The largest sensitivity of θ to M is observed for deflection angles δ which tend to 0, i.e. for Mach waves issuing from a punctual disturbance.

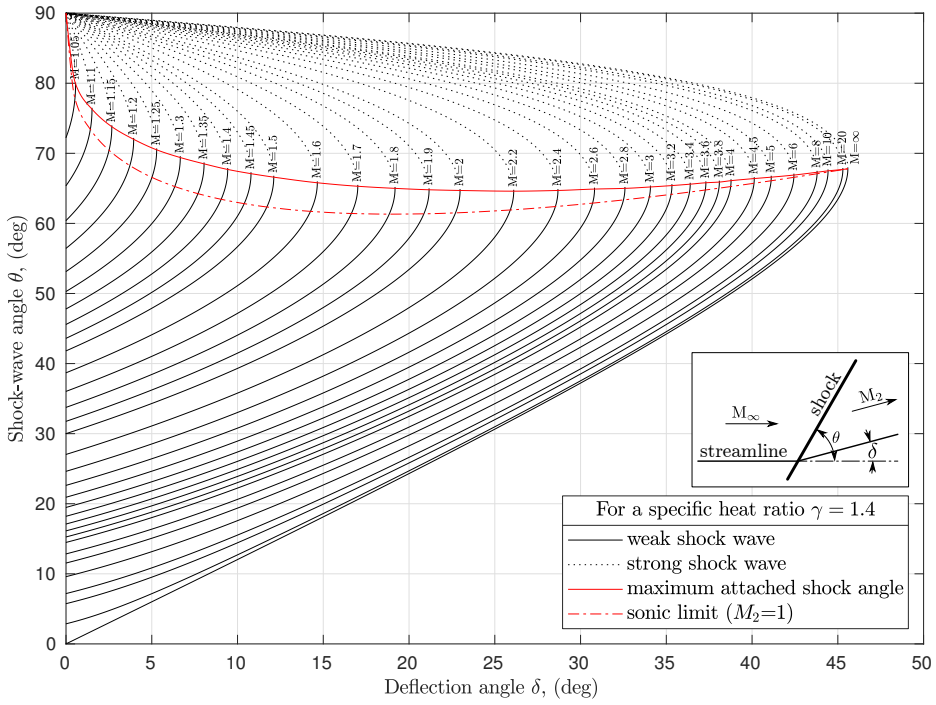

Figure 11: Variation of shock-wave angle with flow-deflection angle for various upstream Mach number ($\gamma = 1.4$).

From a practical point of view, a punctual disturbance in the free-stream of the Longshot could not be generated[2]. The shock waves around a slender static pressure probe provide a useful alternative, especially far

[2]Attempts with laser discharges proved unsuccessful given the low free-stream densities, but additional investigations with laser

downstream of the nosetip where they approach Mach waves. These weak shock waves can be observed using a regular Schlieren flow visualization technique. The viscous effects taking place along the probe actually alter slightly the flow topology and prevent from inferring the free-stream Mach number directly from the shock wave inclination. Instead, the Schlieren images may be compared with numerical results obtained for a given set of free-stream flow conditions (M_∞ and Re_∞). An example is presented in Fig. 12 for a static pressure probe geometrically similar to the one described in §3.3. Boundary conditions imposed at the inlet of the numerical domain match the ones inferred from the methodology described in §4.2 for the time instant corresponding to the experimental image.

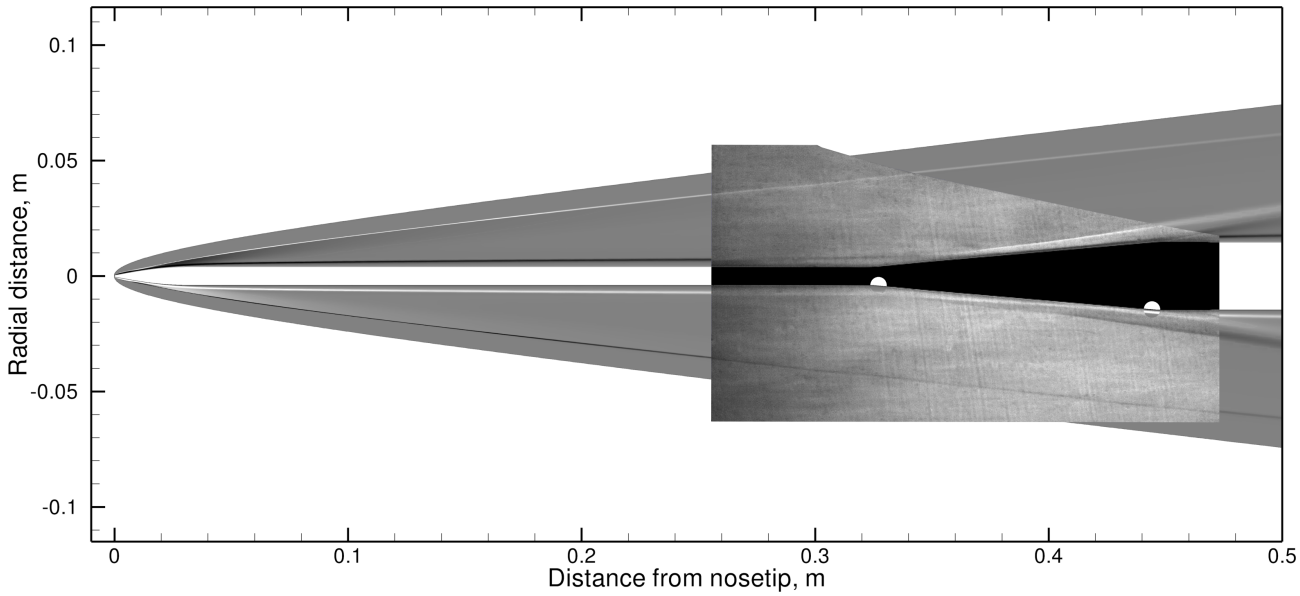

Figure 12: Experimental Schlieren flow visualization around a slender static pressure probe overlapped with a numerical Schlieren (vertical density gradients, free-stream Mach number is 11.6).

The weak shock waves around the probe closely match the position expected from numerical predictions. Shocks issuing from the enlarging base of the probe also match closely the predictions. Overall, the excellent agreement obtained in between the experimental and numerical visualizations supports the accuracy of the free-stream Mach number derived. Higher free-stream Mach numbers would have lead to shock waves significantly closer to the body [25].

Flow visualization along a $800\,\mathrm{mm}$ long slender cone geometry ($7\,^\circ$ half-angle) leads to similar results [19].

5.2 Free-stream static temperature

Determining the translational-rotational temperature, or the vibrational one, is not straightforward for pure nitrogen hypersonic flows. Non-intrusive measurement techniques such as CARS [39–41] seem to be applicable. Until this is implemented in the Longshot wind tunnel, alternative techniques are required to estimate the static temperature of the flow. An indirect method is associated with the detection of the onset of flow condensation, described as follows.

As for other cold-hypersonic wind tunnels, the Longshot is operated at low free-stream static temperatures (typically about $50 - 80\,\mathrm{K}$). This is right above the saturation temperature of nitrogen at the low static pressure

pulses in the picosecond range at high energies might still prove valuable.

involved [42, 43]. By lowering further the free-stream static temperature, flow condensation can in theory be initiated. Recent experiments in the Longshot have gone along this way.

Several experiments have been performed in order to promote the onset of flow condensation. To this end, the Longshot compression process [18] was gradually tuned in order to generate lower stagnation temperatures in the reservoir (while keeping the peak stagnation pressure roughly the same for all experiments). Upon expansion of the flow through the nozzle, lower temperatures in the free-stream could gradually be achieved and flow condensation was ultimately observed. Results are presented in Fig. 13.

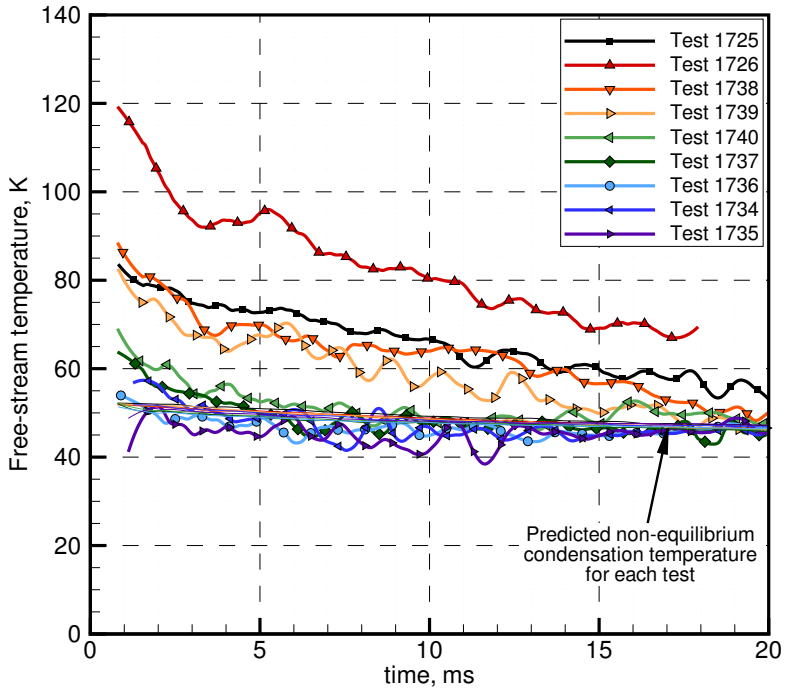

Figure 13: Free-stream static temperature for different experiments in the Longshot wind tunnel (thick lines) [19] and comparison with theoretical condensation temperature (thin lines) [43].

The thick black curve corresponds to the "Medium Reynolds" operating condition of the Longshot. The temporal decay in the free-stream from $80\,\mathrm{K}$ to $55\,\mathrm{K}$ is a typical feature of Longshot experiments, which stems from the decreasing stagnation conditions in the reservoir (as it empties with time). The saturation temperature for nitrogen corresponding to this experiment can be estimated from the literature [42]. The rapid expansion of the flow actually induces non-equilibrium effects which contribute to delay the onset of condensation: this is referred to as supercooling effects. This condensation temperature in non-equilibrium conditions can also be estimated from the literature [43] and is plotted in Fig. 13 using thin colored lines. Actually, the use of contoured nozzles, as in the case of the Longshot, reduces the benefits from supercooling effects because of the relatively small expansion rate parameter associated with these nozzles ($\dot{P} \approx 50$ for the Longshot one). In these conditions, the non-equilibrium condensation temperature (laying in between 50 and $47\,\mathrm{K}$ depending on the free-stream static pressure) is only a few Kelvin lower than the saturation temperature. Looking back at the thick black curve in Fig. 13, one sees that standard Longshot operating conditions always remains above the non-equilibrium condensation temperature threshold.

Additional experiments have been performed with lower stagnation temperature [19, 44]. The corresponding free-stream static temperatures (as rebuilt from the method described in §4.1) is also included in Fig. 13.

The non-equilibrium condensation temperature associated with each of these experiments is also indicated as thin lines. For all these experiments, the rebuilt free-stream static temperature is always reaching a plateau at approximately 50 to $47\,\mathrm{K}$. This close match with the expected non-equilibrium condensation temperature indicates that the free-stream static temperature is correctly determined.

This is of course an indirect free-stream static temperature measurement but the good agreement obtained speaks in favor of the accuracy of the rebuilding approach. It also confirms that standard Longshot operating conditions are free from condensation.

5.3 Free-stream Reynolds number

There exists no probe to measure either a local or free-stream Reynolds number, but this quantity can be inferred indirectly as follows.

The natural boundary layer laminar-to-turbulent transition phenomenon is known to be strongly influenced by the local Reynolds number. Transition locations denoted by x_{tr} are indeed often nondimensionalized and expressed in terms of $\mathrm{Re}_{x_{tr}}$. While experiments in conventional hypersonic wind tunnels (i.e. with large free-stream turbulence levels, as opposed to quiet tunnels [45]) do not enable to compare the transition location itself with flight measurements, they do enable comparisons of the characteristics of the boundary layer instabilities that will lead to transition. In particular, the spectra of the boundary layer instabilities can be compared with Linear Stability Theory (LST) predictions.

Inviscid boundary layer instabilities are usually the most amplified ones for sharp conical geometries at $0\,^\circ$ angle of attack traveling at hypersonic velocities. This has been reported theoretically [46], experimentally [47] and numerically [48]. It has been found that the frequency of the most-amplified boundary layer instabilities scales relatively well with the local boundary layer thickness, which itself depends on the local Reynolds number.

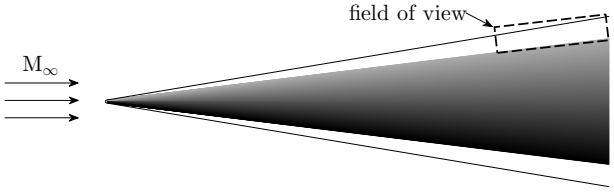

(a) Field of view.

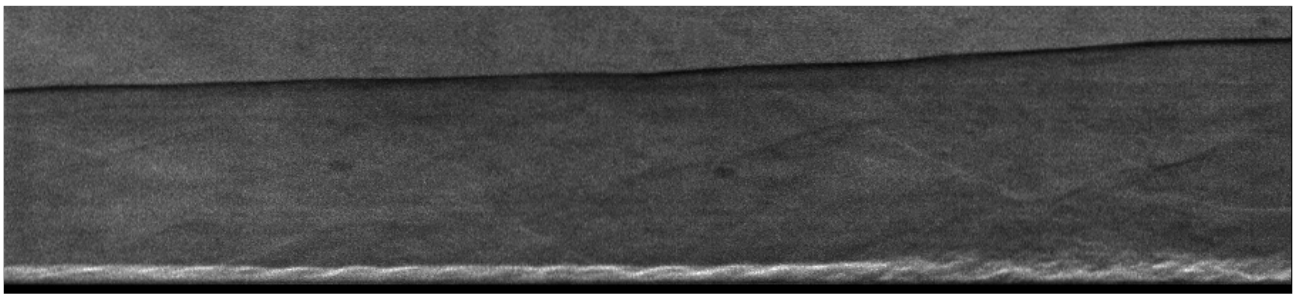

(b) Lif-based Schlieren flow visualization technique [19].

Figure 14: Natural boundary layer instabilities observed along a nearly sharp cone (nosetip radius $R_N = 1.75\,\mathrm{mm}$, $7\,^\circ$ opening half-angle) within Longshot flow conditions [19].

Figure 14 illustrates the natural boundary layer instabilities along a cone placed within the free-stream of the Longshot, as captured using a LIF-based Schlieren setup [49]. The rope-pattern is characteristic of these

instabilities (i.e. the so-called second mode waves) and ultimately leads to transition as visible on the right-hand side of the picture.

These boundary layer instabilities are associated with large pressure fluctuations which can be measured using flush-mounted fast-response pressure sensors. Frequency analysis using wavelet techniques then reveals frequency content which strongly depends upon the instrumented location (plain lines in Fig. 15). An excellent agreement is observed when comparing the peak frequencies[3] with predictions from LST [50]. These LST predictions were obtained from a numerical mean flow solution around the cone, with inlet boundary conditions matching the free-stream flow properties computed by the method described in §4.1 for the time instant at which measurements were performed. If the free-stream Reynolds number had been different, the development of these instabilities would have been altered and different spectra would have been observed (i.e. shifted either to higher or lower frequency ranges). The good agreement again supports the accuracy of the present methodology.

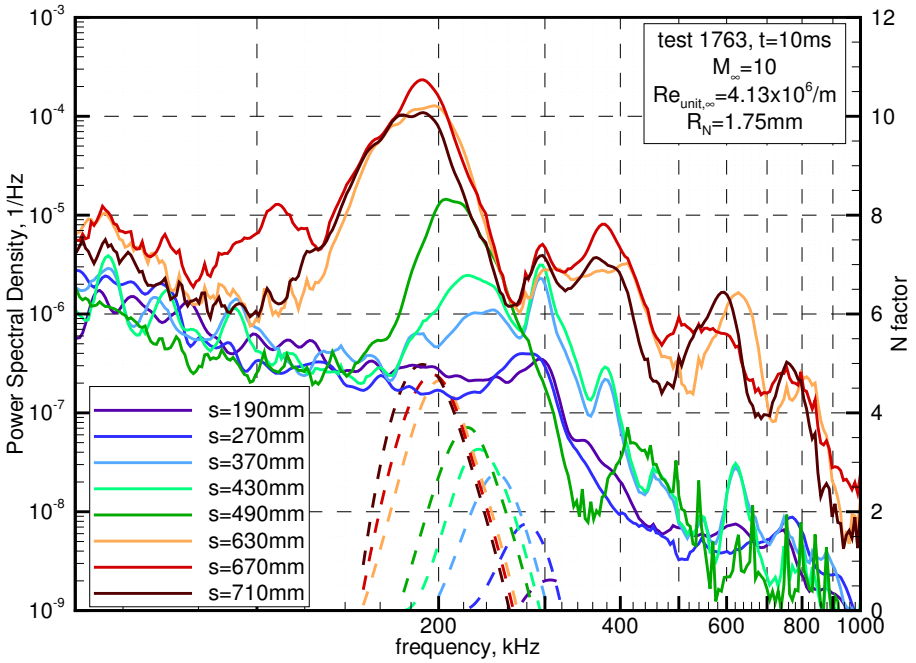

Figure 15: Power spectra of boundary layer instabilities (plain lines) and comparisons with N-factors determined from LST computations (dashed lines) for a 1.75 mm nosetip cone, $\mathrm{M}_\infty = 10$ and $\mathrm{Re}_{\mathbf{unit},\,\infty} = 4.13 \cdot 10^6\ /\mathrm{m}$) [19].

Referring back to Fig. 12, the boundary layer thickness along the probe is also in good agreement with numerical results. This is interpreted as an additional proof for a correctly determined free-stream Reynolds number.

5.4 Free-stream velocity

Velocity measurements in hypersonic flows can be achieved using a wide panel of measurement techniques [51]. In the Longshot wind tunnel, none has been applied recently, but the boundary layer transition experiments reported earlier in §5.3 also offer an indirect approach to evaluate the free-stream velocity.

The group velocity u_c of the natural boundary layer instabilities along the conical experiments highlighted previously can be determined by cross-correlating the pressure signals from the streamwise array of sensors

[3]The amplitudes cannot be compared directly.

and knowing the distance separating them. Alternatively, this group velocity can be estimated from LST theory and is found to be approximately equal to $0.93u_e$ and rather independent of the free-stream flow conditions (u_e being the flow velocity at the edge of the boundary layer). The velocity u_e is nearly equal to the free-stream velocity ($u_e \approx 0.988u_\infty$) as inferred from a Taylor-Maccoll solution for the inviscid flow around a 7° half-angle cone [52]. This yields a theoretical group velocity approximately equal to $0.919u_e$.

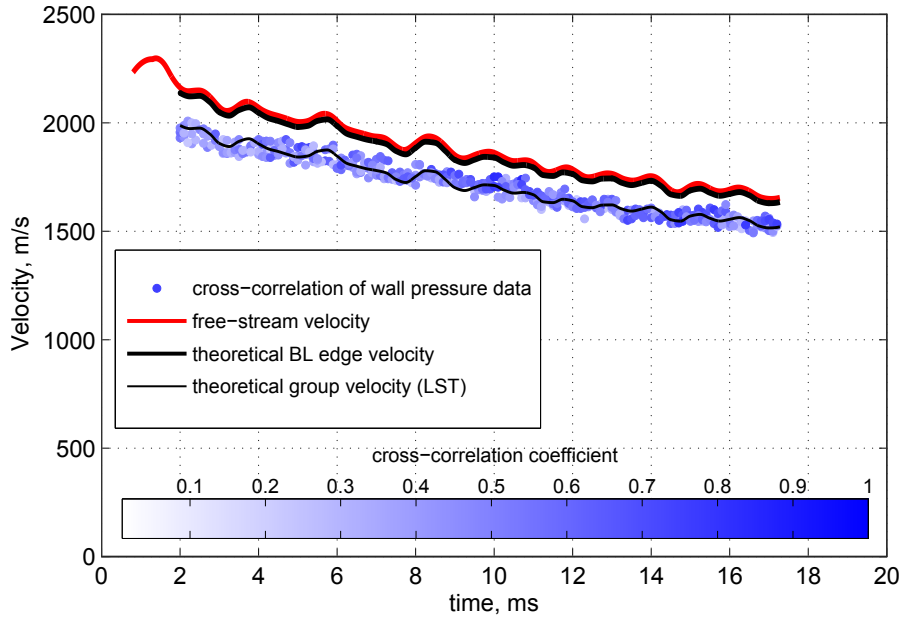

Figure 16: Group velocities for boundary layer instabilities along a cone determined experimentally (Symbols ●), and compared with theoretical predictions (thin line: —) [36].

Experimental measurements and theoretical predictions are presented in Fig. 16 with colored circles and a thin black line, respectively. The excellent agreement observed demonstrates that the free-stream velocity is correctly estimated.

6.0 UNCERTAINTIES ON FREE-STREAM FLOW PROPERTIES

6.1 Accuracy vs. precision

It is important to distinguish between *accuracy* and *precision*: accuracy indicates how close a measurement is to the true value whereas precision indicates how repeatable this measurement can be.

The accuracy is difficult to estimate in the present case since the true value (i.e. the free-stream Mach number, the free-stream total enthalpy...) is not known a priori. Yet, the use of several independent measurement techniques (as reported in §5.0), and the excellent agreement obtained for various flow properties, shows that the systematic errors are probably small for the Longshot case when using the present free-stream rebuilding methodology. The use of a theoretical model which does not require numerous assumptions (such as to describe the nozzle flow expansion) is probably a significant advantage.

The precision (or repeatability) of the present free-stream rebuilding methodology depends on the precision achieved on each of the experimental input (Pitot, stagnation point heat flux and free-stream static pressure).

Former flow characterization methods used for the Longshot [9] were providing a much better precision on some flow properties such as the free-stream Mach number but were also associated with a large bias,

as revealed later on [25]. In this context, it is important to favor the accuracy of a free-stream rebuilding technique rather than its precision: it is indeed the true value of the free-stream flow properties which matters when interpreting data from test articles, rather than the repeatability with which the flow properties can be determined.

Of course, achieving both an accurate and precise determination of flow properties remains the ultimate goal of flow characterization.

6.2 Uncertainties on Longshot free-stream flow properties

Uncertainties on experimental input stem from two contributions: one corresponding to the precision of the measurement itself and another indicating spatial variations across the jet. This was reported in [19] for each experimental input and is summarized as follows:

- The stagnation point heat flux is obtained by integrating a stagnation point temperature history (eq. 1), i.e. a procedure which contributes to decrease precision. It also depends on the thermal product ρck of the material which is difficult to determine accurately. Overall, the precision on the stagnation point heat flux is on the order of $\pm 6\%$.
- The free-stream static pressure remains a difficult measurement in short duration facilities operating at low pressure. This explains a rather poor precision on this input: being on the order of $\pm 7\%$. This can certainly be reduced further in the case of the Longshot.
- The Pitot pressure varies slightly across the hypersonic jet: combining uncertainties on the pressure measurement itself and spatial variation, an overall precision of approximately $\pm 2\%$ is considered.

The corresponding uncertainties on the free-stream flow properties are derived for three of the most common VKI Longshot operating conditions using a perturbation analysis technique. Results are presented in Table 1.

Table 1: Uncertainties on Longshot free-stream flow properties for different operating conditions using the present rebuilding method. Uncertainties stated for a 68.3% confidence interval [19].

		Low Reynolds	Medium Reynolds	High Reynolds
Pitot pressure	p_{t_2}	2.6%	1.6%	1.8%
Stagnation point heat flux	$\dot{q}_w$	6.1%	6.6%	6.1%
Free-stream static pressure	p_∞	7.1%	7.2%	7.7%
Velocity	u_∞	2.4%	2.5%	2.3%
Density	ρ_∞	6.1%	5.7%	5.3%
Static temperature	T_∞	8.8%	8.9%	9%
Total enthalpy	h_{t_∞}	4.8%	5%	4.5%
Mach number	M_∞	3.9%	3.9%	4.2%
Unit Reynolds number	$\mathrm{Re}_{\mathrm{unit},\infty}$	11.1%	11%	10.7%

The largest uncertainties are obtained for parameters such as the free-stream unit Reynolds number. Improving the free-stream static pressure measurements would certainly contribute to reduce these uncertainties. It is also shown that direct free-stream temperature measurements would benefit to the rebuilding process providing their combined accuracy and precision is better than 8.8%.

The free-stream Mach number is mostly sensitive to the free-stream static pressure measurement and that is another justification for improving further the precision of this measurement.

7.0 CONCLUSIONS

The free-stream flow characterization in the VKI Longshot hypersonic wind tunnel has been described in details for the case of nitrogen operation. The methodology follows the one introduced by [10] and focuses on experimental inputs performed within the test section: Pitot, stagnation point heat flux, and static pressure measurements (i.e. excluding measurements from the upstream reservoir). This approach has several advantages: elaborated equations of state are no longer needed; the nozzle flow expansion does not need to be described/modeled.

The original method from [10] has been extended in the present case in order to rigorously solve shock conservation equations while accounting for high-temperature effects. It is applicable to other hypersonic facilities, including the ones operating at higher enthalpies and with other test gases, and is certainly recommended instead of the traditional approaches relying on the assumption of an ideal nozzle flow expansion.

The accuracy of the present rebuilding methodology has been evaluated using different measurement techniques (Schlieren, flow condensation investigations or boundary layer transition experiments, which enable to infer the free-stream Mach number, static temperature, flow velocity and Reynolds number). Overall, the excellent agreement obtained among all these independent approaches demonstrates that accurate free-stream flow properties are determined for the VKI Longshot wind tunnel when assuming free-stream thermal equilibrium. The precision of the method can be improved further, mainly by reducing the uncertainties on the free-stream static pressure measurement.

While independent measurement techniques indicate that Longshot free-stream flow properties are accurately determined, the understanding of the physics taking place during the rapid nozzle flow expansion can certainly be improved further. In particular, thermal non-equilibrium effects need to be addressed: experimental observations support the fact that the flow goes back to an equilibrium state by the time it reaches the nozzle exit, whereas theoretical results indicate that vibrational energy in the free-stream should remain frozen as a result of the rapid flow expansion. Promising non-intrusive diagnostic techniques may bring useful pieces of information.

ACKNOWLEDGMENTS

The authors are thankful to T. Magin for his theoretical and numerical inputs. Warm thanks also go to Z. Ilich for his estimations of the stagnation point velocity gradient in the Longshot flow conditions. Their proofreading and comments have been very much appreciated.

REFERENCES

[1] Span, R., Lemmon, E. W., Jacobsen, R. T., and Wagner, W., "A reference quality equation of state for nitrogen," *International Journal of Thermophysics*, Vol. 19, No. 4, 1998, pp. 1121–1132.

[2] Stollery, J. L. and Smith, J. L., "A note on the variation of vibrational temperature along a nozzle," *Journal of Fluid Mechanics*, Vol. 13, 1962, pp. 225–236.

[3] Kinslow, M. and Miller, J. T., "Nonequilibrium expansion of a diatomic gas through a convergent-divergent nozzle," *The Physics of Fluids*, Vol. 9, No. 9, September 1966, pp. 1703–1708.

[4] Canupp, P. W., Candler, G. V., Perkins, J. N., and Erickson, W. D., "Analysis of hypersonic nozzles including vibrational nonequilibrium and intermolecular force effects," *AIAA Journal*, Vol. 31, No. 7, July 1993, pp. 1243–1249.

[5] Josyula, E. and Bailey, W. F., "Reactive and nonreactive vibrational energy exchanges in nonequilibrium hypersonic flows," *Physics of Fluids*, Vol. 15, No. 10, 2003, pp. 3223–3235.

[6] Perry, R. W., "The Longshot type of high-Reynolds number hypersonic tunnel," *Third hypervelocity techniques symposium*, Advanced experimental techniques for study of hypervelocity flight, March 1964.

[7] Randall, R. E., "Thermodynamic properties of gases: equations derived from the Beattie-Bridgeman equation of state assuming variable specific heats," Technical report AEDC-TR-57-10, GDF, ARO, Inc., August 1957.

[8] Culotta, S. and Richards, B. E., "Methods for determining conditions in real nitrogen expanding flows," Technical Note VKI-TN-58, von Karman Institute for Fluid Dynamics, February 1970.

[9] Simeonides, G., "The VKI hypersonic wind tunnels and associated measurement techniques," Technical Memorandum VKI TM-46, von Karman Institute for Fluid Dynamics, November 1990.

[10] Olivier, H., "An improved method to determine free stream conditions in hypersonic facilities," *Shock Waves*, Vol. 3, No. 3, 1993, pp. 129–139.

[11] Hollis, B. R., "Real-gas flow properties for NASA Langley Research Center aerothermodynamic facilities complex wind tunnels," NASA Contractor Report 4755, NASA Langley Research Center, September 1996.

[12] Marineau, E. C., Lewis, D. R., Smith, M. S., Lafferty, J. F., White, M. E., and Amar, A. J., "Investigation of hypersonic laminar heating augmentation in the stagnation region," *51st AIAA Aerospace Sciences Meeting*, No. AIAA paper 2013-0308, January 2013.

[13] Fay, J. A. and Riddell, F. R., "Theory of stagnation point heat transfer in dissociated air," *Journal of the Aeronautical Sciences*, Vol. 25, No. 2, February 1958, pp. 73–85.

[14] Richards, B. E. and Enkenhus, K. R., "The Longshot free piston hypersonic tunnel," Technical Note 49, von Karman Institute for Fluid Dynamics, September 1968.

[15] Richards, B. E. and Enkenhus, K. R., "Hypersonic testing in the VKI Longshot free-piston tunnel," *AIAA Journal*, Vol. 8, No. 6, June 1970, pp. 1020–1025.

[16] Grossir, G., Ilich, Z., and Chazot, O., "Modeling of the VKI Longshot gun tunnel compression process using a quasi-1D approach," *33rd AIAA Aerodynamic Measurement Technology and Ground Testing Conference*, No. AIAA paper 2017-3985, June 2017.

[17] Ilich, Z., Grossir, G., Paris, S., and Chazot, O., "Experimental investigations of the VKI Longshot gun tunnel compression process," *EUCASS*, No. 155, July 2017.

[18] Grossir, G. and Ilich, Z., "Numerical modeling of the VKI Longshot compression process," *Flow Characterization and Modeling of Hypersonic Wind Tunnels*, No. STO-AVT 325, chap. 2, von Karman Institute for Fluid Dynamics, December 2018.

[19] Grossir, G., *Longshot hypersonic wind tunnel flow characterization and boundary layer stability investigations*, Ph.D. thesis, von Karman Institute for Fluid Dynamics - Université Libre de Bruxelles, July 2015.

[20] Olivier, H., "Thin film gauges and coaxial thermocouples for measuring transient temperatures," Tech. rep., RWTH Aachen, 2000.

[21] Schultz, D. L. and Jones, T. V., "Heat-transfer measurements in short-duration hypersonic facilities," *AGARDograph No. 165*, No. AGARD-AG-165, NATO, February 1973.

[22] Buttsworth, D. R. and Jones, T. V., "Radial conduction effects in transient heat transfer experiments," *The Aeronautical Journal of the Royal Aeronautical Society*, Vol. 101, May 1997, pp. 209–212.

[23] Kindl, H., *Einfluss des Treibergases auf die Strömung in Stosswellenkanälen*, Ph.D. thesis, Rheinisch-Westfälischen Technischen Hochschule Aachen, July 2000.

[24] Grossir, G., Paris, S., Rambaud, P., and Van Hove, B., "Design of static pressure probes for improved free-stream characterization in hypersonic wind tunnels," *52nd AIAA Aerospace Sciences Meeting*, No. AIAA paper 2014-1410, January 2014.

[25] Grossir, G., Van Hove, B., Paris, S., Rambaud, P., and Chazot, O., "Free-stream static pressure measurements in the Longshot hypersonic wind tunnel and sensitivity analysis," *Experiments in Fluids*, Vol. 57, No. 64, May 2016, pp. 1–13.

[26] Magin, T. E., *A model for inductive plasma wind tunnels*, Ph.D. thesis, von Karman Institute for Fluid Dynamics - Université Libre de Bruxelles, June 2004.

[27] Park, C., "Rotational relaxation of N_2 behind a strong shock wave," *Journal of thermophysics and heat transfer*, Vol. 18, No. 4, October-December 2004, pp. 527–533.

[28] Park, C., "The limits of two-temperature model," *48th AIAA Aeeropsace Sciences Meeting*, No. AIAA paper 2010-0911, January 2010.

[29] Vincenti, W. G. and Krüger, C. H., *Introduction to physical gas dynamics*, John Wiley & Sons, 1965.

[30] Bottin, B., Vanden Abeele, D., Magin, T. E., and Rini, P., "Thermodynamic properties of arbitrary perfect gas mixtures at low pressures and high temperatures," *Progress in Aerospace Sciences*, Vol. 36, No. 7, October 2000, pp. 547–579.

[31] Bottin, B., *Aerothermodynamic model of an inductively coupled plasma wind tunnel*, Ph.D. thesis, von Karman Institute for Fluid Dynamics - Université de Liège, October 1999.

[32] Anderson, J. D., *Hypersonic and High Temperature Gas Dynamics*, American Institute of Aeronautics and Astronautics, 2nd ed., 2006.

[33] Grabau, M., Smithson, H. K., and Little, W. J., "A data reduction program for hotshot tunnels based on the Fay-Riddell heat transfer rate using nitrogen at stagnation temperatures from 1500 to 5000K," Tech. Rep. AEDC-TDR-64-50, Arnold Engineering Development Center, June 1964.

[34] Olivier, H., "Influence of the velocity gradient on the stagnation point heating in hypersonic flow," *Shock Waves*, Vol. 5, No. 4, December 1995, pp. 205–216.

[35] Olivier, H., "A theoretical model for the shock stand-off distance in frozen and equilibrium flows," *Journal of Fluid Mechanics*, Vol. 413, June 2000, pp. 345–353.

[36] Ilich, Z., Grossir, G., and Chazot, O., "Evaluation of the stagnation-point velocity gradient in low-enthalpy hypersonic flows," *33rd AIAA Aerodynamic Measurement Technology and Ground Testing Conference*, No. AIAA paper 2017-3984, June 2017.

[37] Liepmann, H. W. and Roshko, A., *Elements of Gasdynamics*, Wiley, 1957.

[38] Ames research staff, "Equations, tables, and charts for compressible flows," Tech. Rep. NACA 1135, NACA, 1953.

[39] Fraval, E., Danehy, P., and Houwing, F., "Single-shot broadband coherent anti-Stokes Raman scattering measurements in a free piston shock tunnel nozzle expansion," *23rd International Symposium on Shock Waves*, July 2001.

[40] Smith, M. S. and Coblish, J. J., "Measurements to assess the degree of thermal nonequilibrium at AEDC hypervelocity tunnel No. 9," *24th AIAA Aerodynamic measurement technology and ground testing conference*, No. AIAA paper 2004-2399, June 2004.

[41] Danehy, P. M., Bathel, B. F., Johansen, C. T., Cutler, A. D., and Hurley, S., "Spectroscopy and spectroscopic: measurement techniques for aerospace flows," *Spectroscopic measurement techniques for aerospace flows*, Lecture Series 2014-06, von Karman Institute for Fluid Dynamics, May 2014.

[42] Wegener, P. P. and Mack, L. M., "Condensation in supersonic and hypersonic wind tunnels," *Advances in applied mechanics*, Vol. 5, chap. 7, Academic Press, Inc., 1958, pp. 307–447.

[43] Daum, F. L. and Gyarmathy, G., "Condensation of air and nitrogen in hypersonic wind tunnels," *AIAA Journal*, Vol. 6, No. 3, March 1968, pp. 458–465.

[44] Grossir, G. and Rambaud, P., "Detection of nitrogen flow condensation onset in a hypersonic wind tunnel using a static pressure probe," *52nd AIAA Aerospace Sciences Meeting*, No. AIAA paper 2014-1153, January 2014.

[45] Schneider, S. P., "Development of hypersonic quiet tunnels," *Journal of Spacecraft and Rockets*, Vol. 45, No. 4, July-August 2008, pp. 641–664.

[46] Mack, L. M., "Boundary layer linear stability theory," *Special course on stability and transition of laminar flows*, No. AGARD 709 in Special course on stability and transition of laminar flows, von Karman Institute for Fluid Dynamics, March 1984, pp. 1–81.

[47] Schneider, S. P., "Hypersonic laminar-turbulent transition on circular cones and scramjet forebodies," *Progress in Aerospace Sciences*, Vol. 40, No. 1-2, February 2004, pp. 1–50.

[48] Li, F., Choudhari, M., Chang, C.-L., and White, J., "Secondary instability of second mode disturbances in hypersonic boundary layers," *RTO AVT-200*, NATO, 2012.

[49] Regert, T., Grossir, G., Paris, S., and Blay Esteban, L., "Schlieren visualization for high-speed flows based on laser-induced fluorescence," *Experiments in Fluids*, Vol. 55, No. 1668, February 2014, pp. 1–6.

[50] Pinna, F., "VESTA toolkit: a software to compute transition and stability of boundary layers," *43rd AIAA Fluid Dynamics Conference*, No. AIAA paper 2013-2616, June 2013.

[51] Boutier, A., Yanta, W. J., and Smeets, G., "Velocity measurements in hypersonic flows: a review," *New trends in instrumentation for hypersonic research*, Vol. 224 of *Applied Sciences*, 1993, pp. 593–602.

[52] Taylor, G. I. and Maccoll, J. W., "The air pressure on a cone moving at high speeds. I," *Proceedings of the Royal Society*, Vol. 139, February 1933, pp. 278–297.